Chapter 1

Advances in Wearable Sensing Technologies and Their Impact for Personalized and Preventive Medicine

Noushin Nasiri and Antonio Tricoli

Additional information is available at the end of the chapter

http://dx.doi.org/10.5772/intechopen.76916

Abstract

Recent advances in miniaturized electronics, as well as mobile access to computational power, are fostering a rapid growth of wearable technologies. In particular, the application of such wearable technologies to health care enables to access more information from the patient than standard episodically testing conducted in health provider centres. Clinical, behavioural and self-monitored data collected by wearable devices provide a means for improving the early-stage detection and management of diseases as well as reducing the overall costs over more invasive standard diagnostics approaches. In this chapter, we will discuss some of the ongoing key innovations in materials science and micro/nanofabrication technologies that are setting the basis for future personalized and preventive medicine devices and approaches. The design of wire- and power-less ultra-thin sensors fabricated on wearable biocompatible materials that can be placed in direct contact with the body tissues such as the skin will be reviewed, focusing on emerging solutions and bottlenecks. The application of nanotechnology for the fabrication of sophisticated miniaturized sensors will be presented. Exemplary sensor designs for the non-invasive measurement of ultra-low concentrations of important biomarkers will be discussed as case studies for the application of these emerging technologies.

Keywords: non-invasive health care, biosensors, wearable electronics

1. Electrochemical sensors

Electrochemical sensors have since long being integrated into microfluidic systems for the measurement of very low concentration of biomarkers [1, 2]. The first electrochemical sensors were developed for oxygen monitoring in the second half of the twentieth century [3]. Miniaturized electrochemical sensors for many toxic gases were commercialized in the 1980s

showing good sensitivity to the permissible exposure limit ranges and selectivity [4]. Compared to optical, mass and thermal sensors, electrochemical sensors are especially attractive because of their remarkable sensitivity, experimental simplicity and low cost [5, 6]. Furthermore, they benefit small power requirements facilitating their integration in small sensing systems. Currently, a variety of electrochemical sensors are being used as detectors in stationary and portable devices for personal safety, clinical, industrial, environmental and agricultural applications [7–9].

Electrochemical detection is usually performed by reducing or oxidizing an electro-active analyte and monitoring the current or potential between the working (WE) and the counter electrodes (CE) as a function of time [5, 6]. As many compounds present relatively easy oxidable or reducible sites, the electrochemical detection mechanism is applicable to a wide number of relevant analytes. There are three main types of electrochemical sensors: potentiometric, amperometric and conductometric [10]. For potentiometric sensors, a local equilibrium is established at the sensor interface, where either the electrode or the membrane potential is measured. The information about the composition of a sample is obtained from the potential difference between two electrodes [11, 12]. Amperometric sensors exploit the use of a potential applied between a reference and a working electrode, to cause the oxidation or the reduction of an electro-active species, which result in currents in a proportional current [13, 14]. Conductometric sensors are based on the measurement of the conductivity at a series of frequencies [15].

Figure 1A shows a schematic of the operation principle of an electrochemical sensor [16]. Commonly, a constant voltage, sufficiently high to initiate the reduction or the oxidation of the analyte, is applied between the working and the counter electrode (**Figure 1A**). The working electrode is usually nanostructured and functionalized with a molecule-specific layer of enzymes or antibodies, providing a selective surface for the redox of the targeted analyte [16, 17]. This results in the rise of a catalytic current between the working and the counter electrode, which is proportional to the analyte concentration [2, 16].

While electrochemistry methods have since long been applied to the characterization of molecules dispersed in liquids, and electrochemical biosensors are commercially available, their integration in wearable sensors is relatively new. In particular, the fabrication of miniaturized electrochemical cells and circuitry that can be placed in close contact with body tissues and related fluids has been challenging. The development of flexible electronic micro-fabrication approaches has enabled the engineering of skin-like planar electrochemical cells that require very small amount of liquids and can be placed on the human skin [18] (**Figure 1B**), iris [6, 19] (**Figure 1C**) and saliva [20] (**Figure 1D**). For instance, the design of functional micro-electrodes on flexible polymer lenses has enabled the online measurement of glucose and other key biomarkers directly from human tears [6, 19] (**Figure 1C**). Typical layouts consist of working (WE), counter (CE) and reference (RE) electrodes [21] deposited on flexible insulating and biocompatible substrates such as 2-methacryloyloxyethyl phosphorylcholine (MPC) polymer [6, 22], polydimethyl siloxane (PDMS) [6, 22] and polyethylene terephthalate (PET) [19]. A current between the working and the counter electrode is generated by targeted redox reactions between the biomarker and the modified working electrode while the opposite reaction takes place at the counter electrode [21, 23]. This results in the generation of an electrochemical

http://dx.doi.org/10.5772/intechopen.76916

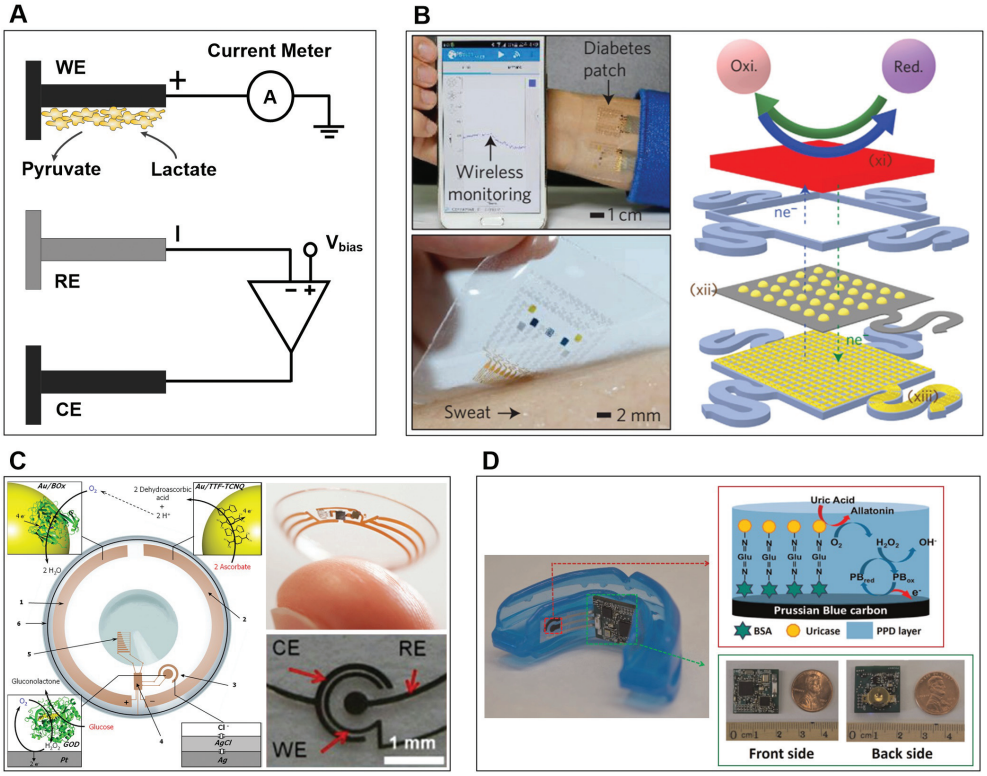

Figure 1. (A) Typical operation principles and sensing mechanisms for electrochemical lactate sensors for other metabolite the functional layer of the working electrode is designed to provide specific bonding and reaction sited to the targeted molecules [73]. Reproduced with permission [73]. Copyright 2017, Wiley Online Library. (B) In-vivo demonstration of a wearable diabetes monitoring and therapeutic system. The electrochemical analyser as an integrated Bluetooth circuit to communicate with external devices (top left). Optical image of the electrochemical sensor array on the human skin collecting perspiration for glucose monitoring (bottom left). Schematic of the GP-hybrid electrochemical unit, which consists of an electrochemically active layers (xi), gold-doped graphene (xii) and a serpentine Au mesh (xiii), from top to bottom (right) [18]. Reproduced with permission [18]. Copyright 2016, Nature Publishing Group. (C) Schematic layout and characterization of a tear glucose electrochemical sensor with an integrated biofuel cell (BFC) on a contact lens [6, 19]. Reproduced with permission [6, 19]. Copyright 2013, ACS Publications, Copyright 2012, Elsevier. (D) Demonstration of a mouthguard biosensor with integrated wireless amperometric circuit board, reagent layer made of a chemically-modified working electrode and the wireless amperometric circuit board: front side and back side [20]. Reproduced with permission [20]. Copyright 2015, Elsevier.

current which, in diluted conditions, is proportional to the concentration of the biomarker [17]. A major advantage is that the selectivity can be enhanced both by coating the nanotexture with highly selective functional groups such as enzymes, antibodies and carefully engineered peptides, and by selecting the appropriate voltage potential for activation of the selected reaction.

Lee et al. [18] reported soft materials, device designs and system integration strategies for a new class of diabetes monitoring and therapy devices based on functionalized chemical vapour deposition (CVD) graphene. Graphene biochemical sensors with solid-state Ag/AgCl

counter electrodes have shown enhanced electrochemical activity, sensitivity and selectivity for the detection of important biomarkers contained in human sweat (**Figure 1B**). Such hybrid interconnections and physical sensors efficiently transmit the signal through the stretchable array and supplement electrochemical sensors, respectively. The orchestrated monitoring of biomarkers and physiological cues with sweat control and transcutaneous drug delivery achieves a closed-loop, point-of-care treatment for diabetes (**Figure 1B**). This demonstrated a stretchable device featuring a serpentine bilayer of gold mesh and gold-doped graphene as an efficient electrochemical interface for the stable transfer of electrical signals. The patch consists of a heater, temperature, humidity, glucose and pH sensors and polymeric microneedles that can be thermally activated to deliver drugs transcutaneously. They showed that the patch can be thermally actuated to deliver Metformin and reduce blood glucose levels in diabetic mice. The diabetes patch is laminated on the human skin and is electrically coupled to a portable electrochemical analyser, which in turn wirelessly transfers data to remote mobile devices and supplies power to the patch (**Figure 1B**). The humidity sensor monitors the increase in RH. It takes about 15 min for the sweat-uptake layer of the patch to collect sweat for the measurement and corresponds to an RH of over 80% [18].

Falk et al. [6] demonstrated a self-powered glucose measurement system based on a miniature biofuel cells (BFCs). It generates ca. 3.1 $\mu W\ cm^{-2}$ of power from the ascorbate and oxygen available in basal tears without influencing the glucose concentration (**Figure 1C**). Calibration and proof of concept were demonstrated ex-situ with a macrocell of 30 mL by chronopotentiometry. Notably, the device showed no sensor response to pure glucose solutions, while a strong electrochemical response was achieved with the addition of ascorbate and ascorbate-dopamine fuels. An open circuit voltage of 0.54 V and a maximal power density of 3.1 $\mu W\ cm^{-2}$ at 0.25 V were measured with human basal tears [6]. These devices showcased a stable current density output of 0.55 $\mu A\ cm^{-2}$ at 0.4 V over 6 h of continuous operation.

Kim et al. [20] presented electrochemical sensors integrated on mouthguards featuring a Bluetooth low-energy communication system for the real-time amperometric monitoring of uric acid (**Figure 1D**). An electrochemical three-electrode layout was screen-printed on the mouthguard and functionalized with a uricase enzyme-modified layer (**Figure 1D**). A 2.45 GHz chip antenna was employed for wireless transmission. These sensors were validated by in vivo measurements of salivary uric acid (SUA) levels in hyperuricaemia patients and healthy individuals. The device was powered with two 1.55 V, 33 mAh watch batteries that were connected in series and consumed in average 21 mW in an active mode and 0.6 mW in a sleep mode. Using a measurement frequency of 60 s enabled battery charge to last up to ca. 5 days. A clear distinction in the SUA levels of the healthy control (178.5 ± 20.7 mM) and hyperuricaemia patients (822.6 ± 26.25 mM) was observed, indicating a good potential of this approach for the diagnostics of hyperuricaemia. A sensitivity of 2.45 mA per mM of uric acid was determined with uric acid solutions with 100–600 mM with an R^2-correlation coefficient of 0.998. Further decreasing the devices size, while reducing power consumption and requirement of integrated batteries may, has the potential to lead to significant commercial applications.

2. Capacitive sensors

Non-contact capacitive sensors work by measuring the changes in capacitance induced by the interaction of a sensing layer with an analyte [24, 25]. When a voltage is applied across two electrodes in an open circuit configuration, an electric field is created between them causing positive and negative charges to collect on the electrode (**Figure 2A**). If the polarity of the voltage is reversed, the charges will also reverse. Usually, capacitive sensors use alternating voltage which causes the charges to continually reverse their positions. The moving of the charges creates an alternating electric current which is strongly influenced by the interaction with the target analyte (**Figure 2B**). More in specific, the current is a function of the capacitance, and the capacitance is determined by the area, proximity of the electrodes and the properties of the space between the electrodes. The larger and closer the electrodes, the higher the current.

Capacitive sensing is becoming increasing popular as an alternative to optical and mechanical sensors for multiple applications such as proximity/gesture detection, material analysis and liquid level sensing. Amongst the advantages of capacitive sensing are its applicability to different kinds of materials such as skin, plastics, metals and liquids, and its contactless and wear-free sensing mechanism, high miniaturization potential, low cost and low-power requirements. Amongst other configurations, capacitive biosensing can be based on capacitive coupling with the human body. This results in a reliable solution for measuring liquid levels (**Figure 2C**) and material composition and creating human-to-machine interfaces such as digital buttons. **Figure 2C–E** displays three basic implementations for capacitive sensing, such as liquid-level sensing (**Figure 2C**), proximity/gesture recognition (**Figure 2D**) and material analysis (**Figure 2E**).

Chen et al. [24] demonstrated low-force capacitive contact lens sensors (**Figure 2F**) for the continuous monitoring of the intraocular pressure (IOP). This is a primary indicative factor in the diagnosis and treatment progress monitoring of glaucoma. The innovative design utilized capacitive sensors for the measurement of these ultra-low pressure variations. To facilitate the wireless transmission of the pressure sensor readings, a curvature-sensing capacitor (C) was coupled with an inductive coil (L) having a fixed inductance resulting in an LC resonant circuit. Changes in the curvature of the soft cornea, and thus in the contact lens electrode spacing, result in variation of the capacitance and resonance frequency of the LC circuit. The resonance frequency was measured wirelessly via a reader integrated in the glass frame worn by the user [26]. The sensing element consisted of a variable gap-sensing capacitor. The electrode with a soft gap was embedded in a soft silicone rubber layer on the corneal side of the lens, while a reference electrode and an inductive coil were fabricated in a hard silicon rubber layer on the outer layer of the lens (**Figure 2F**). The flexible-sensing capacitor was electrically coupled with the hard inductive coil. The sensor lens layout was designed for human eye. For an average person with a cornea radius curvature of 8 mm, the curvature changes due to the typical IOP variation between 5 and 40 mmHg is 0.12 mm for a typical cornea. To maximize the linearity of the sensor response to the pressure change, the difference

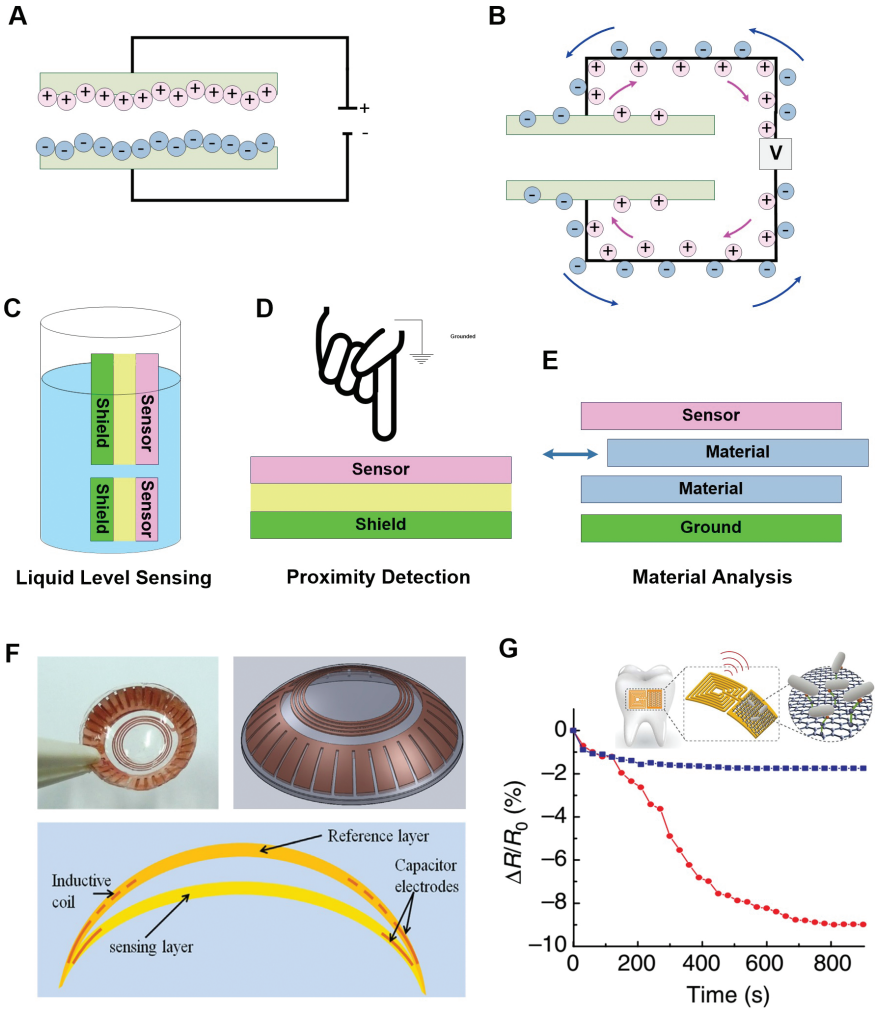

Figure 2. (A) Simplified schematic of conductive sensors: applying a voltage to two electrically insulated electrodes causes positive and negative charges to collect on each side. (B) Applying an alternative voltage causes the charges to move back and forth between the objects, creating an alternating current which is influenced by the space between the electrodes such as the concentration of a target analyte. Basic implements for capacitive sensing: (C) liquid level sensing (parallel fingers), (D) proximity detection (isolated sensor) and (E) material analysis (parallel plate). (F) Capacitive contact lens sensor for IOP monitoring. The sensing element (LC circuit) is embedded into silicone rubber in a double-layer contact lens sensor [24]. Reproduced with permission [24]. Copyright 2013, Elsevier. (G) Biotransfer of the nanosensing architecture onto the surface of a tooth with magnified schematic of the sensing element illustrating wireless readout [25]. Percentage change in graphene resistance versus time following exposure to ~100 H. pylori cells in human saliva (red line). The response to 'blank' saliva solution is shown as blue line [25]. Reproduced with permission [25]. Copyright 2012, Nature Publishing Group.

in radius between the sensing and the reference layers had to be maximized. However, an overly large difference would reduce the IOP sensitivity. A linear, but sufficient range of sensitivity was obtained with a 0.5 mm curvature change for the capacitor. In addition, a circular spiral multi-turn inductive coil designed to have a high quality factor (Q) was used to maximize the reading resolution of the LC resonance circuit.

Mannoor et al. [25] presented a novel approach for passive, wireless, graphene nanosensors to be placed in contact with biomaterials. A biointerfaced-sensing platform, which can be tuned to detect target analytes, was fabricated via silk bioresorption. In particular, they demonstrated their integration onto a tooth for remote monitoring of respiration and bacteria detection in saliva (**Figure 2G**). The architecture consisted of a parallel resonant circuit with a gold inductive coil for wireless transmission and interdigitated capacitive electrodes in contact with graphene-resistive sensors. The resulting system is a passive wireless telemetry device, without the need of on-board power sources and external connections. More in detail, a single-layer, thin-film, inductor-capacitor (LC) resonant circuit integrated in parallel with the resistive graphene monolayer enabled the wireless readout and battery-free operation (**Figure 2G**). The binding of pathogenic bacteria on the graphene nanosensor resulted in variation of its conductance, which induces changes in the characteristic frequencies and bandwidth of sensor resonance (**Figure 2G**). Upon recognition and binding of the specific bacterial targets by the immobilized peptides, the variation of the electrical conductivity of the graphene film was wirelessly monitored using an inductively coupled radio frequency (RF) reader device. The exposure to a 1 μl sample of human saliva containing ~100 *Helicobacter pylori* cells resulted in a real-time variation of the sensor signal as presented in **Figure 2G**. By contrast, 1 μL of "blank" saliva solution without any bacterial cells, used as a control, showed good selectivity and application potential.

3. Chemiluminescence sensors

Luminescence is the emission of light from an electronically excited compound returning to the ground state. The source of excitation energy serves as a basis for a classification of the various types of luminescence and includes electromagnetic waves, heat, friction, electric field or chemical reaction (**Figure 3A**). When the energy source for the excitation is a chemical reaction, this phenomenon is called chemiluminescence (CL). Chemiluminescence measurements usually consist of monitoring the rate of production of photons, which in turn depends on the rate of the luminescent reaction [27, 28]. The light intensity is directly proportional to the concentration of the limiting reactant involved in the luminescence reactions. Thanks to the achievement in miniaturized and integrated optical-sensing systems, very low levels of light intensity can be measured allowing the development of very sensitive analytical methods and systems. Chemiluminescence-based sensors have been then developed with the aim of combining the selective of light-emitting reactions with the convenience of electronic sensors. More recently, chemi- and electrochemiluminescence (ECL) detections have also been used instead of fluorescence for the development of biochips and microarrays.

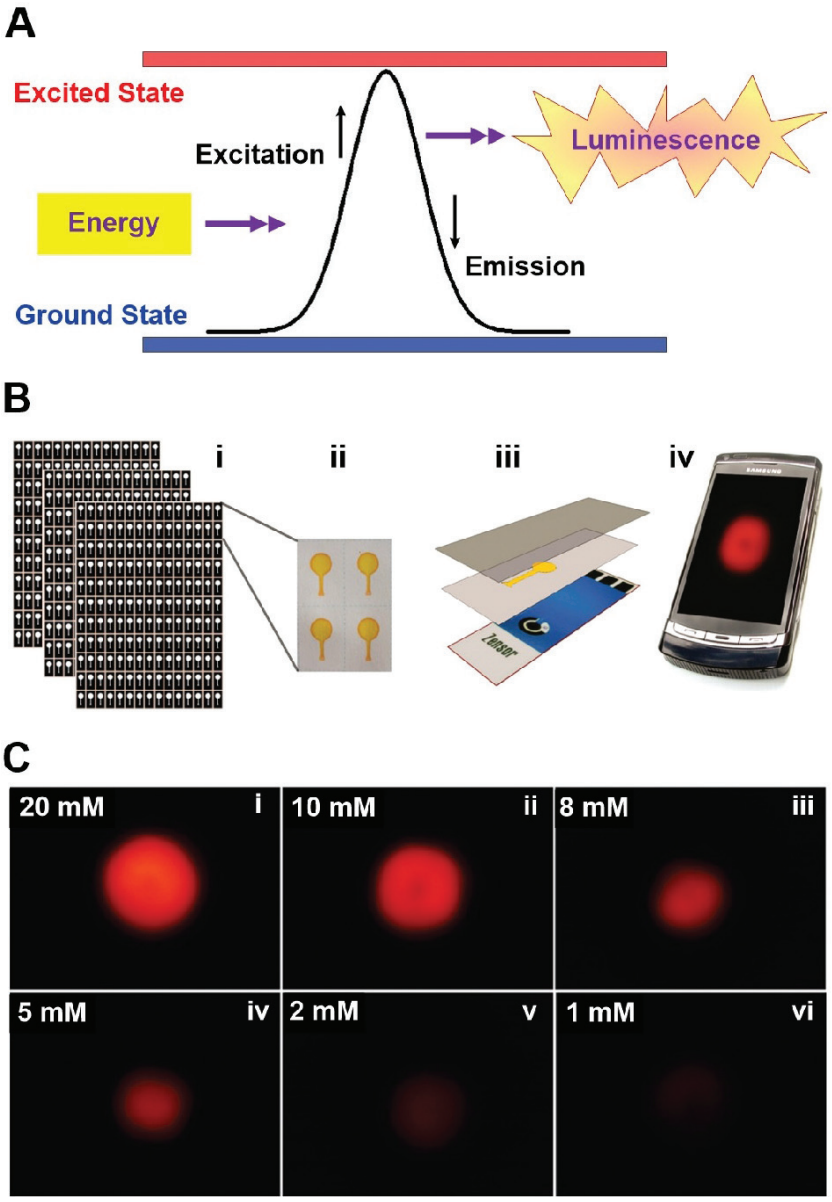

Figure 3. (A) Schematic of luminescence phenomenon consisting in the emission of light from an electronically excited compound returning to the ground state. (B) Fabrication and operation of a paper-based microfluidic ECL sensor [31]. Upon full wetting of the sensing area, the sensor is placed in proximity of the lens of the camera phone and a potential of 1.25 V is applied [31]. The resulting emission is captured and analysed (C) Digital photographic images of ECL emission obtained with various DBAE concentrations (1–20 mM) using a camera phone [31]. The ECL reactions were initiated by stepping the potential from 0 to 1.25 V upon application of a sample droplet [31]. Reproduced with permission [31]. Copyright 2011, ACS Publications.

Freeman and Seitz reported in 1978 the first CL sensor for hydrogen peroxide measurement [29]. Since then, various types of CL-based sensors have been commercially implemented and are extensively used for the analysis of inorganic, organic and biological/pharmaceutical compounds [30]. In recent years, a higher sensitivity of CL-based sensors over other photoluminescence-based ones has attracted significant research focus. The high sensitivity of CL-based sensing is attributed to the suppression of the noise introduced light scattering. Furthermore, CL-based devices feature a simpler set-up with lower background emissions than other photoluminescence detection systems. One of the major remaining deficiencies in the application of CL sensors to routine analysis systems is the short lifetime and signal drift, caused by the irreversible consumption of the CL reagents. While many CL sensors have designs based on the recycling of the CL reagents, which are usually bound to polymers and have a decreased consumption of the luminescent reagent, the stability of this type of sensors is compromised by the bleaching of the reagents or they partition into hydrophobic regions of the film over time.

Recently, Delaney et al. [31] presented an ECL sensor based on paper-based microfluidic devices. Low cost, disposable ECL sensors were fabricated with inkjet-printed paper fluidic substrates and screen-printed electrodes (**Figure 3B**). Such devices can be read with a conventional photodetector or a mobile camera phone. Importantly, because ECL is performed in the dark, unlike the case of colorimetric detection, it is independent of ambient light. The paper fluidic element was placed in direct contact with a screen-printed electrode and tightly enclosed in clear plastic (**Figure 3B**) [31]. A limit of detection of 0.9 μM was achieved with a linear response between 3 μM and 5 mM using a photomultiplier tube as the photodetector. Quantitative results could also be collected using a mobile camera phone by analysing the red intensity from digital images of the ECL emission, using a simple program that can be run on the mobile phone itself. **Figure 3C** shows the photographic images of the ECL emission from the sensors for a range of concentrations of 2-(Dibutylamino)ethanol (DBAE) between 1 and 20 mM, produced by stepping the potential from 0 to 1.25 V. The images reveal an unambiguous relationship between concentration and the intensity of the colour. The red pixel intensity was analysed for each image and a numerical value associated with each intensity was obtained [31].

4. Chemiresistive sensors

Semiconductor-based chemiresistive sensors are amongst the most investigated and widely used devices for the detection of combustible and toxic gases owing to their low cost, miniaturization potential and circuit simplicity [32, 33]. Such chemiresistive gas sensors are able to detect a wide variety of reactive reducing or oxidizing gases at very low ppb concentrations via a strong variation of their resistivity, which are not detectable with catalytic combustion and electrochemical-based gas sensors [34, 35]. A major challenge is their inherent non-specificity, which makes it challenging to use for the identification of unknown and complex gas mixtures. Chemiresistor gas sensors mainly operate on the basis of surface reactions, which cause change in the electrical resistance due to the modulation of the surface charge layer and semiconductor band bending [36]. These types of sensors feature excellent sensitivity, short response time, low cost, and very good suitability for the integration in miniaturized portable instruments making them appealing for numerous applications including breath analysis,

alarm systems and electronic nose [34–36]. In spite of their numerous benefits, chemiresistive sensors have shown different challenges with respect to their commercialization such as poor reproducibility, long-time instability due to aging of the sensing materials and surfaces, cross-sensitivity to other gases and also to water vapour [37, 38].

Chemiresistive-type sensors using various semiconducting metal oxides, such as WO_3, MoO_3, SnO_2 and NiO, have been demonstrated for use as exhaled breath sensors, due to their superior sensitivity to volatile organic compounds (VOCs) and integration in portable devices [38–42]. A major requirement is the development of selective semiconductor material and surface that can provide fast response times [43]. Here, the sensing mechanism of chemiresistive devices is schematically described in **Figure 4A** and **B**. Oxygen molecules physisorb on the oxide surface, with electrons being transferred from the metal oxide to the oxygen which is ionosorbed [44, 45]. Several oxygen species are adsorbed including molecular (O_2) and atomic (O, O_2) ions with their fraction depending from the operating temperature (**Figure 4A** and **C**). These adsorbed ions scatter electrons within the Debye length (d) of the metal oxide forming a depleted region (**Figure 4B** and **C**), and band bending, with a reduced electron mobility near the oxide surface [44, 46].

The reception function of a common chemiresistive semiconductor, such as SnO_2 (in air) for a reducing or oxidizing analyte, consists of the variation of the ionosorbed oxygen concentration [44, 47]. If a reducing analyte is injected in the sensing chamber, such as EtOH, H_2 or CO, the surface concentration of oxygen ions is decreased (**Figure 4B**), releasing some of the trapped electrons back to the semiconductor and reducing the concentration of the scattering centres. As a result, the electron mobility and carrier concentration of the semiconductor are increased [38, 44]. In more detail, the ionosorbed oxygen scatters electrons within the Debye length of SnO_2, reducing its electron mobility. For large grains ($d_p > > \delta$), the sensing mechanism is controlled by the grain boundaries (**Figure 4C**). For ultra-fine nanoparticles, there are two possible mechanisms as a function of the grain size (d_p) [44, 46, 48]. If the grain size is larger than twice the Debye length, a conduction channel with bulk mobility exists within a diameter ($L_C = d_p - 2\delta$) from the grain centre (**Figure 4C**) [46, 49, 50]. A change in the scattering centre concentration (O_2, O, O_2) will then only result in a change in the conduction channel width (L_C). By contrast, if the grain is smaller or equal to twice d, then the whole grain is depleted (**Figure 4C**); therefore, a reduction of the ionosorbed oxygen may 'open' a conduction channel through the oxide (**Figure 4C**) [49, 51].

Recently, Moon et al. [41] present a high-performance chemiresistive electronic nose (CEN) based on an array of metal oxide semiconductor thin films, metal-catalysed thin films and nanostructured thin films. It consisted of differently nanostructured thin films based on metal oxides, including tungsten trioxide (WO_3), tin dioxide (SnO_2) and indium oxide (In_2O_3) (**Figure 4D**). These nanostructured thin films were synthesized by e-beam deposition in a glancing angle deposition. The chemiresistive-sensing properties of these nine sensing element arrays were explored for the diagnostics of asthma, halitosis and kidney disorders. The CEN operating at 168°C demonstrated a sensitive and selective detection of NO, H_2S and NH_3 with an 80% relative humidity (RH) atmosphere (**Figure 4E**). The estimated detection limits of this sensor array for these gas molecules were in the sub-ppb range, suggesting their potential use

http://dx.doi.org/10.5772/intechopen.76916

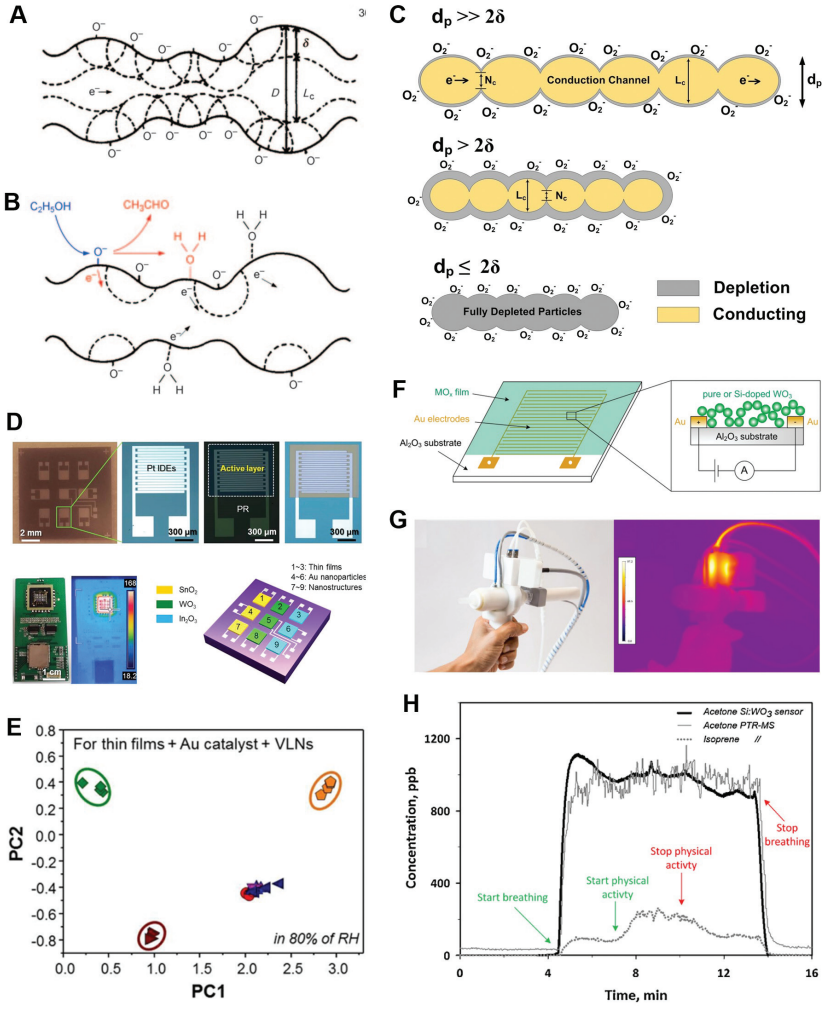

Figure 4. Schematic model of the chemiresistive sensing mechanism of semiconductor metal oxides based on the oxygen ionosorption on the semiconductor surface in (A) pure dry air and (B) with ethanol [44]. Reproduced with permission [44]. Copyright 1982, AIP Publishing. (C) As a function of the ratio between the particle diameter (d_p) and the Debye length (δ), three sensing mechanisms are expected [46]. (Reproduced with permission [46]. Copyright 2015, Wiley Online Library. (D) Optical microscope images of the sequential fabrication process of the CEN on a single chip (1 × 1 cm) containing an active layer (1 × 1 mm) on Pt interdigitated electrodes [41]. Reproduced with permission [41]. Copyright 2016, ACS Publications. (E) PCA plot showing the responses to 8 gases with 80% RH [41]. (F) Detector schematic: a metal oxide (MO_x) film is deposited onto a sensor substrate consisting of an Al_2O_3 support with interdigitated Au electrodes [55]. Reproduced with permission [55]. Copyright 2010, ACS Publications. (G) Picture of the operating hand-held sampler and sensing unit with a disposable mouthpiece (left). IR camera image (right) confirmed the absence of any hot-spots close to the mouth piece or holder, the temperatures are always below 40°C there [52]. Reproduced with permission [52]. Copyright 2015, IOP Publishing. (H) Estimated acetone concentration with the Si:WO_3 sensor (thick solid line) and acetone (thin solid line) and isoprene (dotted line) concentrations measured by PTR-MS during breath analysis of a healthy subject during physical activity [39]. Reproduced with permission [39]. Copyright 2012, Elsevier.

for the diagnosis of asthma, halitosis and kidney disease via breath analysis. The enhanced sensitivity of these sensing materials is attributed to the spill-over effect of the noble metal Au nanoparticle catalysts and the high porosity of villi-like nanostructures, which provides a large surface-to-volume ratio. Using principal component analysis (PCA), the CEN can detect and distinguish the H_2S, NH_3 and NO biomarkers in exhaled breath (**Figure 4E**).

Righettoni et al. [39, 52] developed a portable acetone sensor (**Figure 4F** and **G**) consisting of flame-deposited [53, 54] and in situ-annealed, Si-doped epsilon-WO_3 nanostructured films, capable of measuring ultra-low acetone concentrations (down to 20 ppb) with a high signal-to-noise ratio in ideal (dry air) and realistic (up to 90% RH) conditions. The detector films consist of highly sensitive and selective pure and Si-doped WO_3 nanoparticle films (10–13 nm in diameter) made of the gas phase and aerosol-deposited onto interdigitated electrodes [55] as previously demonstrated for SnO_2, ZnO and Si-SnO_2 nanoparticles [43, 56–58]. The breath acetone content of test persons was monitored continuously and compared to that measured via proton transfer reaction mass spectrometry (PTR-MS). Notably, in addition to providing similar breath acetone concentration readings to the PTR-MS and a better signal-to-noise ratio, the chemiresistive sensor response times were below 15 s, making these devices attractive for breath analysis (**Figure 4H**). Acetone concentrations of 20 ppb were measured with high signal-to-noise ratios above 10. Furthermore, the sensor response was robust against variation in gas flow rates down to 0.2 $L.min^{-1}$, facilitating the application of such sensors for real breath measurement devices.

5. pH-monitoring sensors

Monitoring of chronic wounds is a relatively unexplored area that presents significant challenges to modern health-care providers. Chronic wounds are defined as wounds that either do not heal or heal very slowly or may reoccur after healing. Generally, wounds that do not heal within 3 months are termed chronic [59]. They affect more than nine million people across the United States and Europe with an annual cost exceeding US$ 39 billion [60, 61]. Usually, diabetic, obese and elderly people tend to suffer from chronic wounds [62, 63]. Untimely, treatment may lead rapidly to infections and complications. The diagnosis and the treatment of chronic wounds are quite complex, providing a major challenge to the health-care staff [64]. One of the major causes of disruption of the healing process, which may lead to a chronic wound, is bacterial infection which may result in the overgrowth of a newly formed capillary-rich granulation tissue over the wound [65]. This condition, termed as over-granulation, can hamper the healing process and may result in a protruding, friable flesh that is very sensitive and bleeds easily.

There is currently no commercially available wireless device to continuously monitor the wound-healing process. Patients rely on medical staff for physical inspection of the wound, which requires repeated trips to clinics or prolonged hospitalization. Few devices have been reported in the study that monitor parameters related to the wound-healing process. These include a bandage in a solution form that can be painted onto the skin to form a thin film [66].

http://dx.doi.org/10.5772/intechopen.76916

The film emits oxygen-dependent phosphorescence that can be used to map the oxygen levels of the underlying skin tissue. In another example, a flexible electrode array has been developed through the inkjet printing of gold nanoparticle on flexible polyethylene naphthalate to measure the impedance spectrum of the tissues for early detection of pressure ulcers [67]. Electrodes have been demonstrated to measure moisture levels [68] as well as bacteria [69] in wound dressings. Changes in pH values have also been related to the presence of infection. An infected wound shows slightly basic pH due to certain enzyme activities, bacterial colonization and formation of protein structures [70]. However, these approaches rely on the sensing of a single parameter to monitor the wound-healing process, while the healing is a complex process that may require information about a number of factors affecting the wound healing. An attractive solution would be the integration of low cost, wearable, compact, wireless, real-time wound-monitoring system on the adhesive bandages that are commonly used to protect wounds from the external environment. Such a system could be worn by patients everyday and be able to issue early warnings to the patients regarding any abnormality in the healing process, as well as wirelessly send the data recordings of multiple parameters related to the wound-healing process to the remote medical staff.

Recently, Farooqui et al. [71] reported a wearable system to wirelessly monitor chronic wounds using simple bandage strips. The system comprised a set of inkjet-printed sensors on a disposable bandage to monitor bleeding, pH levels and external pressure on the wound site. The sensor and wireless circuitry electronics were integrated on the bandage in a reusable fashion, thus maintaining the disposability of the bandage strip in contact with the wound (**Figure 5A–C**). This wearable bandage could alert the patient and the health-care providers regarding any abnormality in the wound-healing process through the integrated wireless module [71]. The pH levels on the wound site were detected by changes in resistance of one of the electrodes (carbon-based) placed on the bandage [71]. The wireless tests were performed while the bandage is worn on the body as shown in **Figure 5C**. A fluid was injected underneath the bandage using a narrow tube, attached to a syringe containing the fluid, imitating a wound-bleeding process. A Zigbee wireless receiver was placed to receive an information signal from the bandage. When the fluid was pumped from the syringe and reaches the bottom side of the bandage, the transmitter on the bandage was activated and sent information to the receiver [71].

Guinovart et al. [72] demonstrated a wearable potentiometric pH cell embedded into an adhesive bandage for real-time monitoring of pH variations in a wound. Screen-printed silver-silver chloride electrodes were deposited on a commercial adhesive bandage forming a potentiometric cell. The fabrication process is illustrated in **Figure 5D**. A transparent dielectric insulator was first printed onto the cellulose pad to cover the area where the potentiometric electrodes would be printed [72]. Then, conductive traces that defined the electrode underlayer were made by screen-printing of an Ag/AgCl conductive ink. Thereafter, a carbon layer was overlaid on the traces to fabricate the working electrode. Finally, an insulator ink was used to shield the conductive tracks and expose the electro-active areas and contact pads for micro-wiring [72]. To assess the ability of the sensor to dynamically monitor pH changes in wounds, a poly(ethylene glycol) (PEG) hydrogel, cured on top of both electrodes, was used to emulate a healing segment of tissue. **Figure 5E** shows a typical pH time response. First, a sharp decrease in the pH is observed. This corresponds to the diffusion of the supplied solution to the

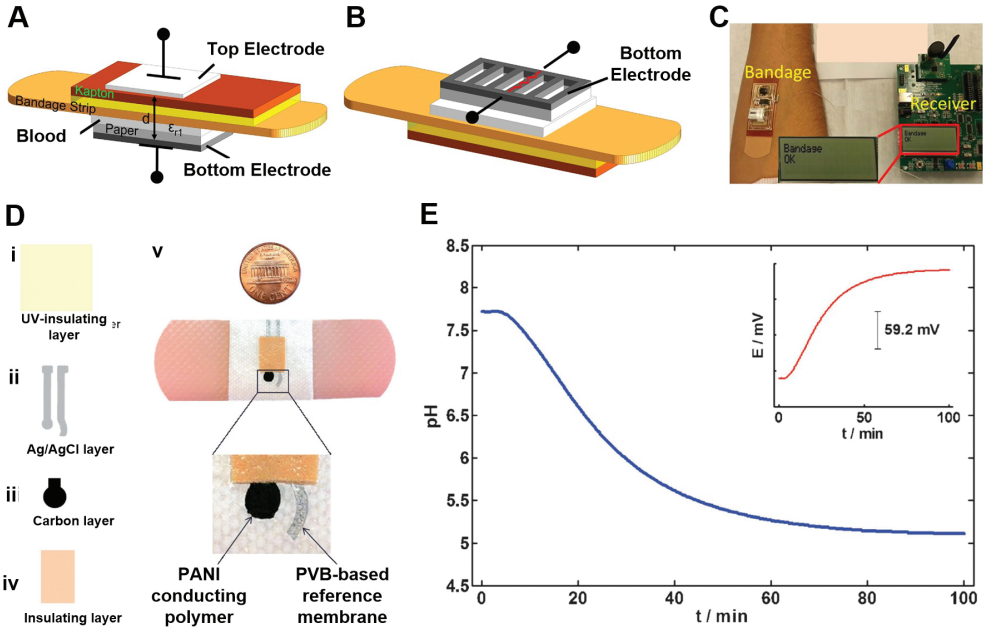

Figure 5. (A) Two sensor electrodes are mounted on the top and the bottom side of a bandage forming a capacitor. (B) The pH levels are sensed when the resistance of the carbon based bottom electrode changes in response to the pH levels. (C) The bandage (with exposed electronics) is worn on the forearm [71]. Reproduced with permission [71]. Copyright 2016, Nature Publishing Group. (D) Fabrication process for a pH-sensing bandage device. (i–iv) An insulating layer is printed, followed by an Ag/AgCl and a carbon layer, and finally an insulating layer with skin-like colour. (v) Images displaying the printed potentiometric sensor on an adhesive bandage [72]. Reproduced with permission [72]. Copyright 2014, Wiley Online Library. (E) Real-time recording of pH changes over a 100-min interval using a PEG hydrogel simulating the composition of a wound [72].

electrode surface. After 40 min, the pH reaches a similar value to the added solution pH level. The corresponding electromotive force (EMF) profile is shown in the inset of **Figure 5E**. These findings demonstrate that the new pH-sensitive bandage is able to detect pH fluctuations at a wound site with relatively long time intervals (up to 100 min).

6. Conclusions

Advanced wearable-sensing technologies have the potential to offer a minimally intrusive telemedicine platform for individual health service and dramatically alter the landscape of health-care delivery as well as our understanding of many diseases. In this chapter, we have reviewed some recent achievements in miniaturised sensor technologies for the non-invasive detection of disease biomarkers for medical diagnostics. We have classified these technologies according to their working principles and detecting mechanisms. Notably, the development of portable devices is rapidly revolutionising the device layout, resulting in the engineering of

wearable sensor systems on tattoos, bandages and contact lenses. Highly selective body fluid sensors for readily available sweat, saliva and tears have been developed leveraging on existing electrochemical, capacitive and pH-monitoring technologies, which can benefit from an extensive library of enzymes for biomolecule detection. Similarly, non-invasive breath analysis approaches based on solid-state devices made of unique nanomaterial compositions can sense important biomarkers such as acetone, one the primary breath markers for diabetes, down to a few particles per billion. By enhancing reducing health-care costs and providing novel health data with unprecedented frequency, these smart wearable sensors can play a critical role in revolutionising the future health-care system and improving our quality of life.

Acknowledgements

A.T. gratefully acknowledges the support of Australian Research Council DP150101939, Australian Research Council DE160100569 and Westpac2016 Research Fellowship.

Conflict of interest

The authors have no conflict of interest to declare.

Author details

Noushin Nasiri[1] and Antonio Tricoli[2]*

*Address all correspondence to: antonio.tricoli@anu.edu.au

1 Faculty of Science, Institute for Biomedical Materials and Devices, University of Technology Sydney, Sydney, NSW, Australia

2 Nanotechnology Research Laboratory, Research School of Engineering, Australian National University, Canberra, Australia

References

[1] Xu S, Zhang Y, Jia L, Mathewson KE, Jang K-I, Kim J, et al. Soft microfluidic assemblies of sensors, circuits, and radios for the skin. Science. 2014;**344**(6179):70-74. DOI: 10.1126/science.1250169

[2] Jia W, Bandodkar AJ, Valdés-Ramírez G, Windmiller JR, Yang Z, Ramírez J, et al. Electrochemical tattoo biosensors for real-time noninvasive lactate monitoring in human perspiration. Analytical Chemistry. 2013;**85**(14):6553-6560. DOI: 10.1021/ac401573r

[3] Zhu W, Bao C, Li F, Zhou X, Yang J, Yu T, et al. An efficient planar-heterojunction solar cell based on wide-bandgap $CH_3NH_3Pb_{I2}.1Br_{0.9}$ perovskite film for tandem cell application. Chemical Communications. 2016;**52**(2):304-307. DOI: 10.1039/C5CC07673K

[4] Stetter JR, Zaromb S, Penrose WR. Sensor Array for Toxic Gas Detection. Google Patents; 1987

[5] Kim J, Jeerapan I, Imani S, Cho TN, Bandodkar A, Cinti S, et al. Noninvasive alcohol monitoring using a wearable tattoo-based Iontophoretic-biosensing system. ACS Sensors. 2016;**1**(8):1011-1019. DOI: 10.1021/acssensors.6b00356

[6] Falk M, Andoralov V, Silow M, Toscano MD, Shleev S. Miniature biofuel cell as a potential power source for glucose-sensing contact lenses. Analytical Chemistry. 2013;**85**(13):6342-6348. DOI: 10.1021/ac4006793

[7] Li H, Mu X, Yang Y, Mason AJ. Low power multimode electrochemical gas sensor Array system for wearable health and safety monitoring. IEEE Sensors Journal. 2014;**14**(10):3391-3399. DOI: 10.1109/JSEN.2014.2332278

[8] Tang L, Zeng G-M, Shen G-L, Li Y-P, Zhang Y, Huang D-L. Rapid detection of Picloram in agricultural field samples using a disposable Immunomembrane-based electrochemical sensor. Environmental Science & Technology. 2008;**42**(4):1207-1212. DOI: 10.1021/es7024593

[9] Hayat A, Marty J. Disposable screen printed electrochemical sensors: Tools for environmental monitoring. Sensors. 2014;**14**(6):10432. DOI: 10.3390/s140610432

[10] Bakker E, Telting-Diaz M. Electrochemical sensors. Analytical Chemistry. 2002;**74**(12):2781-2800. DOI: 10.1021/ac0202278

[11] Schazmann B, Morris D, Slater C, Beirne S, Fay C, Reuveny R, et al. A wearable electrochemical sensor for the real-time measurement of sweat sodium concentration. Analytical Methods. 2010;**2**(4):342-348. DOI: 10.1039/B9AY00184K

[12] Guinovart T, Parrilla M, Crespo GA, Rius FX, Andrade FJ. Potentiometric sensors using cotton yarns, carbon nanotubes and polymeric membranes. The Analyst. 2013;**138**(18):5208-5215. DOI: 10.1039/C3AN00710C

[13] Yin Z, Wu J, Yang Z. Amperometric sensors based on Ni/Al and co/Al layered double hydroxides modified electrode and their application for hydrogen peroxide detection. Biosensors & Bioelectronics. 2011;**26**(5):1970-1974. DOI: 10.1016/j.bios.2010.08.049

[14] Yang Y-L, Chuang M-C, Lou S-L, Wang J. Thick-film textile-based amperometric sensors and biosensors. The Analyst. 2010;**135**(6):1230-1234. DOI: 10.1039/B926339J

[15] Li D, Hu J, Wu R, Lu JG. Conductometric chemical sensor based on individual CuO nanowires. Nanotechnology. 2010;**21**(48):485502. DOI: 10.1088/0957-4484/21/48/485502

[16] Kharitonov SA, Barnes PJ. Biomarkers of some pulmonary diseases in exhaled breath. Biomarkers. 2002;**7**(1):1-32. DOI: 10.1080/13547500110104233

[17] Bollella P, Fusco G, Tortolini C, Sanzò G, Favero G, Gorton L, et al. Beyond graphene: Electrochemical sensors and biosensors for biomarkers detection. Biosensors & Bioelectronics. 2016;**89**:152-166. DOI: 10.1016/j.bios.2016.03.068

[18] Lee H, Choi TK, Lee YB, Cho HR, Ghaffari R, Wang L, et al. A graphene-based electrochemical device with thermoresponsive microneedles for diabetes monitoring and therapy. Nature Nanotechnology. 2016;**11**:566. DOI: 10.1038/nnano.2016.38

[19] Thomas N, Lähdesmäki I, Parviz BA. A contact lens with an integrated lactate sensor. Sensors and Actuators B: Chemical. 2012;**162**(1):128-134. DOI: 10.1016/j.snb.2011.12.049

[20] Kim J, Imani S, de Araujo WR, Warchall J, Valdés-Ramírez G, Paixão TRLC, et al. Wearable salivary uric acid mouthguard biosensor with integrated wireless electronics. Biosensors & Bioelectronics. 2015;**74**:1061-1068. DOI: 10.1016/j.bios.2015.07.039

[21] Wang W-S, Kuo W-T, Huang H-Y, Luo C-H. Wide dynamic range CMOS Potentiostat for Amperometric chemical sensor. Sensors. 2010;**10**(3):1782. DOI: 10.3390/s100301782

[22] Chu MX, Miyajima K, Takahashi D, Arakawa T, Sano K, Sawada S-I, et al. Soft contact lens biosensor for in situ monitoring of tear glucose as non-invasive blood sugar assessment. Talanta. 2011;**83**(3):960-965. DOI: 10.1016/j.talanta.2010.10.055

[23] Azzouzi S, Rotariu L, Benito AM, Maser WK, Ali MB, Bala C. A novel amperometric biosensor based on gold nanoparticles anchored on reduced graphene oxide for sensitive detection of L-lactate tumor biomarker. Biosensors & Bioelectronics. 2015;**69**:280-286. DOI: 10.1016/j.bios.2015.03.012

[24] Chen G-Z, Chan I-S, Lam DCC. Capacitive contact lens sensor for continuous non-invasive intraocular pressure monitoring. Sensors & Actuators, A: Physical. 2013;**203**:112-118. DOI: 10.1016/j.sna.2013.08.029

[25] Mannoor MS, Tao H, Clayton JD, Sengupta A, Kaplan DL, Naik RR, et al. Graphene-based wireless bacteria detection on tooth enamel. Nature Communications. 2012;**3**:763. DOI: 10.1038/ncomms1767

[26] Schnakenberg U, Walter P, vom Bögel G, Krüger C, Lüdtke-Handjery HC, Richter HA, et al. Initial investigations on systems for measuring intraocular pressure. Sensors and Actuators, A: Physical. 2000;**85**(1):287-291. DOI: 10.1016/S0924-4247(00)00426-X

[27] Liu X, Freeman R, Golub E, Willner I. Chemiluminescence and chemiluminescence resonance energy transfer (CRET) aptamer sensors using catalytic hemin/G-quadruplexes. ACS Nano. 2011;**5**(9):7648-7655. DOI: 10.1021/nn202799d

[28] Li LL, Liu KP, Yang GH, Wang CM, Zhang JR, Zhu JJ. Fabrication of graphene–quantum dots composites for sensitive electrogenerated chemiluminescence immunosensing. Advanced Functional Materials. 2011;**21**(5):869-878. DOI: 10.1002/adfm.201001550

[29] Freeman TM, Seitz WR. Chemiluminescence fiber optic probe for hydrogen peroxide based on the luminol reaction. Analytical Chemistry. 1978;**50**(9):1242-1246. DOI: 10.1021/ac50031a012

[30] Zhang Z, Zhang S, Zhang X. Recent developments and applications of chemiluminescence sensors. Analytica Chimica Acta. 2005;**541**(1–2):37-46. DOI: 10.1016/j.aca.2004.11.069

[31] Delaney JL, Hogan CF, Tian J, Shen W. Electrogenerated chemiluminescence detection in paper-based microfluidic sensors. Analytical Chemistry. 2011;**83**(4):1300-1306. DOI: 10.1021/ac102392t

[32] Whitfield MD, McKeag RD, Pang LY, Chan SS, Jackman RB. Thin film diamond UV photodetectors: Photodiodes compared with photoconductive devices for highly selective wavelength response. Diamond and Related Materials. 1996;**5**(6–8):829-834. DOI: 10.1016/0925-9635(95)00419-X

[33] Pacholski C, Kornowski A, Weller H. Self-assembly of ZnO: From nanodots to nanorods. Angewandte Chemie, International Edition. 2002;**41**(7):1188-1191. DOI: 10.1002/1521-3773(20020402)41:7<1188::AID-ANIE1188>3.0.CO;2-5

[34] Mirica KA, Azzarelli JM, Weis JG, Schnorr JM, Swager TM. Rapid prototyping of carbon-based chemiresistive gas sensors on paper. Proceedings of the National Academy of Sciences of the United States of America. 2013;**110**(35):E3265-E3E70. DOI: 10.1073/pnas.1307251110

[35] Ramgir N, Datta N, Kaur M, Kailasaganapathi S, Debnath AK, Aswal DK, et al. Metal oxide nanowires for chemiresistive gas sensors: Issues, challenges and prospects. Colloids and Surfaces, A: Physicochemical and Engineering Aspects. 2013;**439**:101-116. DOI: 10.1016/j.colsurfa.2013.02.029

[36] Meng F-L, Guo Z, Huang X-J. Graphene-based hybrids for chemiresistive gas sensors. Trends in Analytical Chemistry. 2015;**68**:37-47. DOI: 10.1016/j.trac.2015.02.008

[37] Fratoddi I, Venditti I, Cametti C, Russo MV. Chemiresistive polyaniline-based gas sensors: A mini review. Sensors and Actuators, B: Chemical. 2015;**220**:534-548. DOI: 10.1016/j.snb.2015.05.107

[38] Tricoli A, Righettoni M, Teleki A. Semiconductor gas sensors: Dry synthesis and application. Angewandte Chemie, International Edition. 2010;**49**(42):7632-7659. DOI: 10.1002/anie.200903801

[39] Righettoni M, Tricoli A, Gass S, Schmid A, Amann A, Pratsinis SE. Breath acetone monitoring by portable Si:WO_3 gas sensors. Analytica Chimica Acta. 2012;**738**:69-75. DOI: 10.1016/j.aca.2012.06.002

[40] Righettoni M, Tricoli A, Pratsinis SE. Thermally stable, silica-doped ε-WO_3 for sensing of acetone in the human breath. Chemistry of Materials. 2010;**22**(10):3152-3157. DOI: 10.1021/cm1001576

[41] Moon HG, Jung Y, Han SD, Shim Y-S, Shin B, Lee T, et al. Chemiresistive electronic nose toward detection of biomarkers in exhaled breath. ACS Applied Materials & Interfaces. 2016;**8**(32):20969-20976. DOI: 10.1021/acsami.6b03256

[42] Moon HG, Shim Y-S, Kim DH, Jeong HY, Jeong M, Jung JY, et al. Self-activated ultrahigh chemosensitivity of oxide thin film nanostructures for transparent sensors. Scientific Reports. 2012;**2**:588. DOI: 10.1038/srep00588

[43] Zayasu K, Sekizawa K, Okinaga S, Yamaya M, Ohrui T, Sasaki H. Increased carbon monoxide in exhaled air of asthmatic patients. American Journal of Respiratory and Critical Care Medicine. 1997;**156**(4):1140-1143. DOI: 10.1164/ajrccm.156.4.96-08056

[44] Ogawa H, Nishikawa M, Abe A. Hall measurement studies and an electrical conduction model of tin oxide ultrafine particle films. Journal of Applied Physics. 1982;**53**(6):4448-4455. DOI: 10.1063/1.331230

[45] Harrison PG, Willett MJ. Tin oxide surfaces. Part 20—Electrical properties of tin (IV) oxide gel: Nature of the surface species controlling the electrical conductance in air as a function of temperature. Journal of the Chemical Society, Faraday Transactions. 1989;**85**(8):1921-1932. DOI: 10.1039/F19898501921

[46] Nasiri N, Bo R, Wang F, Fu L, Tricoli A. Ultraporous Electron-depleted ZnO nanoparticle networks for highly sensitive portable visible-blind UV Photodetectors. Advanced Materials. 2015;**27**(29):4336-4343. DOI: 10.1002/adma.201501517

[47] Barsan N, Weimar U. Understanding the fundamental principles of metal oxide based gas sensors; The example of CO sensing with SnO_2 sensors in the presence of humidity. Journal of Physics Condensed Matter. 2003;**15**(20):R813. DOI: 10.1088/0953-8984/15/20/201

[48] Nasiri N, Bo R, Hung TF, Roy VAL, Fu L, Tricoli A. Tunable band-selective UV-Photodetectors by 3D self-assembly of heterogeneous nanoparticle networks. Advanced Functional Materials. 2016;**26**(40):7359-7366. DOI: 10.1002/adfm.201602195

[49] Nasiri N, Bo R, Fu L, Tricoli A. Three-dimensional nano-heterojunction networks: A highly performing structure for fast visible-blind UV photodetectors. Nanoscale. 2017; **9**(5):2059-2067. DOI: 10.1039/C6NR08425G

[50] Jesenak M, Banovcin P, Havlicekova Z, Dobrota D, Babusikova E. Factors influencing the levels of exhaled carbon monoxide in asthmatic children. The Journal of Asthma. 2014; **51**(9):900-906. DOI: 10.3109/02770903.2014.936448

[51] Nasiri N, Bo R, Chen H, White TP, Fu L, Tricoli A. Structural engineering of Nano-grain boundaries for low-voltage UV-Photodetectors with gigantic photo- to dark-current ratios. Advanced Optical Materials. 2016;**4**(11):1787-1795. DOI: 10.1002/adom.201600273

[52] Righettoni M, Ragnoni A, Güntner AT, Loccioni C, Pratsinis SE, Risby TH. Monitoring breath markers under controlled conditions. Journal of Breath Research. 2015;**9**(4):047101. DOI: 10.1088/1752-7155/9/4/047101

[53] Nasiri N, Elmoe TD, Liu Y, Qin QH, Tricoli A. Self-assembly dynamics and accumulation mechanisms of ultra-fine nanoparticles. Nanoscale. 2015;**7**(21):9859-9867. DOI: 10.1039/C5NR00877H

[54] Yahuitl Osorio M, The D, Noushin N, Thomas PW, Antonio T, Kylie RC. Flame-made ultra-porous TiO_2 layers for perovskite solar cells. Nanotechnology. 2016;**27**(50):505403. DOI: 10.1088/0957-4484/27/50/505403

[55] Righettoni M, Tricoli A, Pratsinis SE. Si:WO_3 sensors for highly selective detection of acetone for easy diagnosis of diabetes by breath analysis. Analytical Chemistry. 2010; **82**(9):3581-3587. DOI: 10.1021/ac902695n

[56] Tricoli A, Graf M, Mayer F, Kuühne S, Hierlemann A, Pratsinis SE. Micropatterning layers by flame aerosol deposition-annealing. Advanced Materials. 2008;**20**(16):3005-3010. DOI: 10.1002/adma.200701844

[57] Tricoli A, Graf M, Pratsinis SE. Optimal doping for enhanced SnO_2 sensitivity and thermal stability. Advanced Functional Materials. 2008;**18**(13):1969-1976. DOI: 10.1002/adfm.200700784

[58] Tricoli A, Nasiri N, Chen H, Wallerand AS, Righettoni M. Ultra-rapid synthesis of highly porous and robust hierarchical ZnO films for dye sensitized solar cells. Solar Energy. 2016; **136**:553-559. DOI: 10.1016/j.solener.2016.07.024

[59] Nunan R, Harding KG, Martin P. Clinical challenges of chronic wounds: Searching for an optimal animal model to recapitulate their complexity. Disease Models & Mechanisms. 2014;**7**(11):1205-1213. DOI: 10.1242/dmm.016782

[60] Sen CK, Gordillo GM, Roy S, Kirsner R, Lambert L, Hunt TK, et al. Human skin wounds: A major and snowballing threat to public health and the economy. Wound Repair and Regeneration. 2009;**17**(6):763-771. DOI: 10.1111/j.1524-475X.2009.00543.x

[61] Posnett J, Gottrup F, Lundgren H, Saal G. The resource impact of wounds on health-care providers in Europe. Journal of Wound Care. 2009;**18**(4):154. DOI: 10.12968/jowc.2009.18.4.41607

[62] Gist S, Tio-Matos I, Falzgraf S, Cameron S, Beebe M. Wound care in the geriatric client. Clinical Interventions in Aging. 2009;**4**:269. DOI: 10.2147/CIA.S4726

[63] Blakytny R, Jude E. The molecular biology of chronic wounds and delayed healing in diabetes. Diabetic Medicine. 2006;**23**(6):594-608. DOI: 10.1111/j.1464-5491.2006.01773.x

[64] Hampton S. Understanding overgranulation in tissue viability practice. British Journal of Community Nursing. 2007;**12**(Sup4):S24-S30. DOI: 10.12968/bjcn.2007.12.Sup4.43000

[65] Gardner SE, Frantz RA, Doebbeling BN. The validity of the clinical signs and symptoms used to identify localized chronic wound infection. Wound Repair and Regeneration. 2001;**9**(3):178-186. DOI: 10.1046/j.1524-475x.2001.00178.x

[66] Li Z, Roussakis E, Koolen PG, Ibrahim AM, Kim K, Rose LF, et al. Non-invasive transdermal two-dimensional mapping of cutaneous oxygenation with a rapid-drying liquid bandage. Biomedical Optics Express. 2014;**5**(11):3748-3764. DOI: 10.1364/BOE.5.003748

[67] Swisher SL, Lin MC, Liao A, Leeflang EJ, Khan Y, Pavinatto FJ, et al. Impedance sensing device enables early detection of pressure ulcers in vivo. Nature Communications. 2015;**6**: 6575. DOI: 10.1038/ncomms7575

[68] Kim I-Y, Suh S-H, Lee I-K, Wolfe RR. Applications of stable, nonradioactive isotope tracers in in vivo human metabolic research. Experimental & Molecular Medicine. 2016;**48**(1): e203. DOI: 10.1038/emm.2015.97

[69] McColl D, Cartlidge B, Connolly P. Real-time monitoring of moisture levels in wound dressings in vitro: An experimental study. International Journal of Surgery. 2007;**5**(5):316-322. DOI: 10.1016/j.ijsu.2007.02.008

[70] Schreml S, Szeimies RM, Karrer S, Heinlin J, Landthaler M, Babilas P. The impact of the pH value on skin integrity and cutaneous wound healing. Journal of the European Academy of Dermatology and Venereology. 2010;**24**(4):373-378. DOI: 10.1111/j.1468-3083.2009.03413.x

[71] Farooqui MF, Shamim A. Low cost inkjet printed smart bandage for wireless monitoring of chronic wounds. Scientific Reports. 2016;**6**:28949. DOI: 10.1038/srep28949

[72] Guinovart T, Valdés-Ramírez G, Windmiller JR, Andrade FJ, Wang J. Bandage-based wearable potentiometric sensor for monitoring wound pH. Electroanalysis. 2014;**26**(6): 1345-1353. DOI: 10.1002/elan.201300558

[73] Tricoli A, Nasiri N, De S. Wearable and miniaturized sensor technologies for personalized and preventive medicine. 2017;**27**(15):1605271. DOI: 10.1002/adfm.201605271